JOURNAL OF MATERIALS SCIENCE 37 (2002) 353–363

Fabrication of a new class of porous media models for visualization studies of multiphase flow processes

C. D. TSAKIROGLOU*, D. G. AVRAAM‡
Institute of Chemical Engineering and High Temperature Chemical Processes, Foundation for Research and Technology, Hellas (ICE/HT-FORTH), Stadiou Str.-Platani, P.O. Box 1414, GR-26500 Patras, Greece
E-mail: ctsakir@iceht.forth.gr

The conventional wet-chemistry techniques used for the fabrication of porous media models exhibit some shortcomings with regard to the control of the structural parameters of pores etched either on glass or on plastic plates. A new method of fabrication of pore network micro-models, using an excimer laser LIGA technique, is presented. First, the microstructure is etched on a thin PMMA layer by using as input data the pore depth distribution (10–25 μm) and the pore width-to-depth aspect ratio distribution ($\sim$1–4). Then, the void space is filled with a layer of nickel (total thickness$\sim$300 μm) which, in turn, is covered by a thick layer of copper ($\sim$1700 μm) by using micro-electroforming. Finally, and after a series of mechanical treatments, a metal insert, which is a negative replica of the target microstructure, is produced and used for the printing of a large number of identical structures on PMMA plates with hot embossing. Each plastic model is glued with a thin PMMA cover foil by using a spin coating technique. In this manner, pore network models of well-controlled pore dimensions are produced. It is found that the depth of pores is well-controlled, whereas the depth of each intersection region (node) is almost equal to the sum of the depths of the two intersected capillaries (bonds). The aforementioned features in combination with the broad pore depth and width range (10–100 μm) make the new micro-models representative of real porous media such as natural formations (e.g. sedimentary rocks, soils). Preliminary experiments of two-phase immiscible displacement performed on the new models confirm their applicability to visualization studies of multiphase transport processes in porous media.

1. Introduction

Multi-fluid transport processes in porous media are encountered in a wide variety of practical applications either of industrial interest, such as the oil and gas recovery from underground rock reservoirs [1–5], or of environmental significance, such as the risk assessment & in situ remediation of soils and aquifers contaminated by agricultural chemicals, landfill leachates, industrial wastes, etc [6, 7]. Porous media models, that is pore networks etched in glass or plastic have been used in numerous visualization studies of multiphase transport processes (e.g. two- and three-phase immiscible displacement) in order to clarify the pore-scale mechanisms [8–17], identify the mesoscopic patterns of fluid distribution [17, 18–22], and determine the dependence of mesoscopic transport coefficients (e.g. residual saturation of fluids at the end points, two-phase relative permeabilities, drainage/imbibition capillary pressure curves, etc) on microstructural parameters of pores, fluid properties and process dynamics [8, 15, 18, 21, 23, 24]. Furthermore, such experimental studies became the basis for the development and evaluation of pore network simulators for multiphase transport processes [19–21, 25, 26].

In general, pore networks constructed with wet-chemistry techniques are unable to retain certain structural properties of real porous media [11, 16, 20]. Specifically, (a) the pore depth is not a well-controlled parameter and is usually adjusted by changing the duration of glass etching and sintering, (b) the variability of the pore depth (which is the smallest dimension) is very low and (c) the pore dimensions are relatively high ($>$50 μm). These built-in characteristics of pore network models result in relatively low values of capillary pressure, high mean value ($\sim$100 μm) and small variation of the equivalent capillary diameter distribution, as

*Author to whom all correspondence should be addressed.
‡*Present Address*: CPERI-CERTH, P.O. Box 361, GR-57001 Thermi – Thessaloniki, Greece.

well as in small (∼1–1.2) chamber-to-throat equivalent capillary diameter aspect ratio [8, 11, 16]. In addition, the precise reproduction of a structure in many copies is difficult to be attained with chemical or photo etching techniques, and models constructed from the same pattern (mask) always exhibit certain differences caused by small variations in exposure times [8, 11, 16]. The pore structure of natural porous formations (e.g. sedimentary rocks such as sandstones and carbonates, soils, etc) is characterized by wide pore size distributions, medium and large values of chamber to throat diameter aspect ratio (∼2–10) and mean pore sizes ranging from 100 μm to lower than 0.1 μm [27].

The objective of the present work is the construction of pore network models by using an excimer laser ablation technique, in order to avoid all above-mentioned shortcomings of the conventional models. In this manner, multiple identical micro-models, which are representative of real porous media (e.g. natural formations), are expected to be constructed. Such models will enable us to perform visualization multiphase transport experiments under realistic conditions.

2. Fabrication of micro-models

Pore network models can be constructed either by etching directly the final micro-structure on a plate with an excimer laser ablation technique or by using a series of moulding/replication processes (laser-LIGA technique) [28]. In the first case, the direct production of a large number of identical micromodels requires the iterative operation of the excimer laser for a long period under unaltered conditions. Such a procedure is economically inefficient and exceptionally time-consuming. In the second case, the excimer laser ablation technique is used just once for the etching of the structure on a thin plastic layer and then micro-electroforming produces a metal insert, which is a metallic negative replica of the microstructure (laser-LIGA technique). This metal insert can be used for the fabrication of an enormous multitude of identical microstructures on plastic plates with high precision, by using either hot embossing or injection moulding techniques. Obviously, the excimer laser-LIGA process [28] is much cheaper than a direct method and allows the production of a great number of identical microstructures. This is particularly important for the case of pore network models intended to be used iteratively in multiphase flow experiments. The basic steps of the excimer laser LIGA process, that was used for the fabrication of pore network micromodels are described in the following.

1. Initially, the dimensions of the pores are selected and the laser is programmed for the construction of the microstructure (Fig. 1). The characteristics of the target structure are fed as input data to the laser computer. The

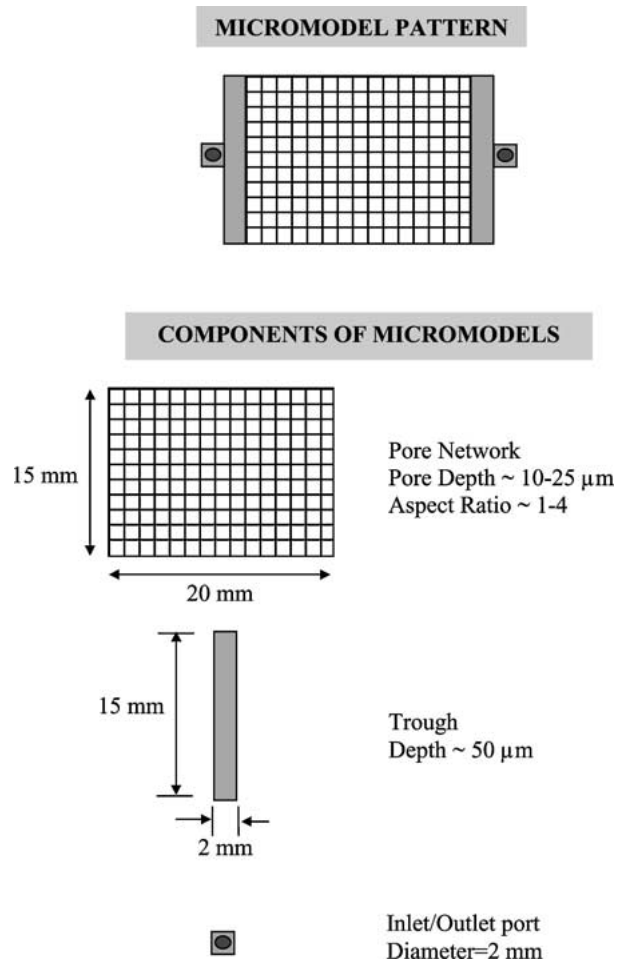

Figure 1 Structural characteristics of pore network micromodels.

TABLE I Pore-depth and pore width-to-depth aspect ratio distributions

Depth (μm)	Frequency	Aspect ratio	Frequency
Input pore-depth and pore width-to-depth aspect ratio distributions			
10	0.2	1.0	0.15
15	0.3	2.0	0.35
20	0.3	3.0	0.35
25	0.2	4.0	0.15
Mean depth = 17.7 μm		Mean aspect ratio = 2.5	
St. Dev. of depth = 10.5 μm		St. Dev of asp.ratio = 0.92	
Selected pore-depth and pore width-to-depth aspect ratio distributions			
10	0.203	1.0	0.174
15	0.260	2.0	0.304
20	0.348	3.0	0.348
25	0.189	4.0	0.174
Mean depth = 17.6 μm		Mean aspect ratio = 2.52	
St. Dev. of depth = 9.14 μm		St. Dev of asp.ratio = 0.945	

pattern of the microstructure is a square network that consists of 39 columns × 30 rows of straight pores of constant length (500 μm), variable depth (10–25 μm) and variable width to depth aspect ratio (1–4). The dimensions of the network are 20 mm × 15 mm, whereas each column (x-axis) and each row (y-axis) is characterized by constant pore depth and width which are selected randomly from pre-specified discrete size distributions (Table I). Given that the total number of columns and rows is quite small (=69) the statistical distributions of the selected pore dimensions (Table I) are expected to differ slightly from the input ones. Two troughs of dimensions 15 mm × 2 mm and depth 50 μm are placed as inlet and outlet ports to ensure uniform

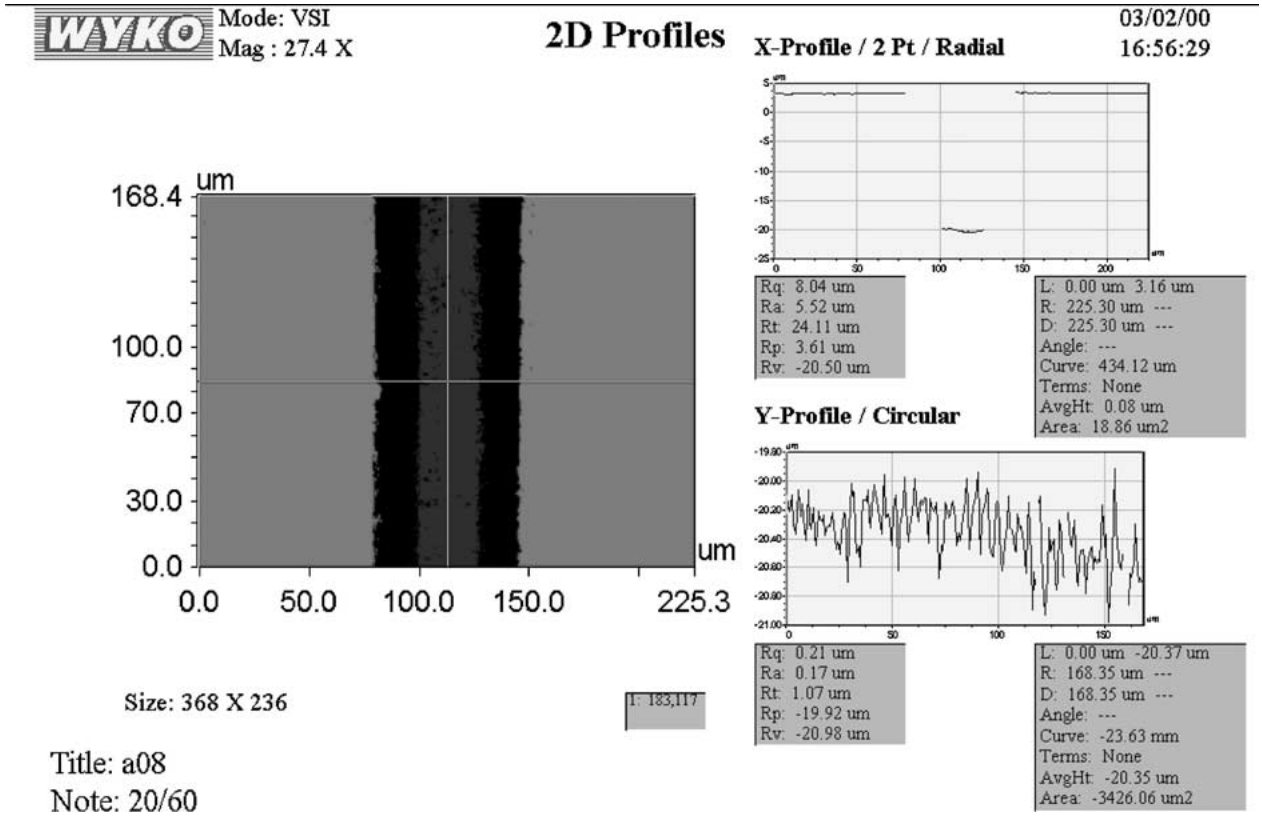

Figure 2 Measurement of the pore depth of micromodels with the aid of the program WYKO from pictures of UV-Interferometry. The depth is almost uniform (∼23 μm) along the pore cross-section (x-axis profile) and exhibits very low variation (<1 μm) along the pore length (y-axis profile).

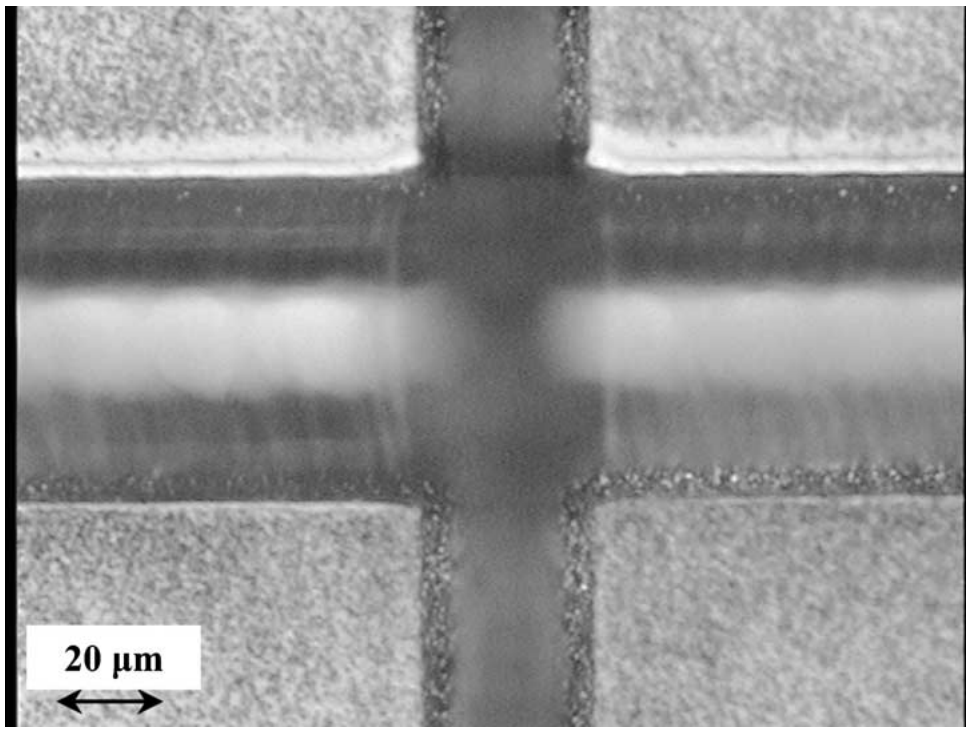

Figure 3 Detail of the intersection region between one column and one row of the pore network.

and homogeneous fluid distribution outside the network (Fig. 1). The communication of the microstructure with external fluid sinks is ensured through two large holes placed close to the troughs (Fig. 1).

2. A titanium wafer of diameter 10 cm is covered with liquid PMMA monomer that is thermally polymerized. Afterwards, the surface is mechanically polished with a thickness tolerance better than 10 μm. The thickness of the formed polymer layer is about 300 μm. The pore network model is etched on the surface of the polymer layer by excimer laser ablation [28]. The rate of material removal depends on the type of material, the pulse energy and the number of pulses (wavelength = 193 nm). Since the process is controlled by a computer, the operational parameters of the excimer laser are properly adjusted to be consistent with the pore depths and widths.

3. Microelectroforming is used to produce a micromould insert [28]. First, the surface of PMMA is sputter coated with a thin film of titanium ($\sim$50 nm) and silver ($\sim$150 nm) to become electrically conductive. Then, a layer of pure nickel is deposited on the etched structure using as an electrolyte, a solution of nickel sulphamate, boric acid and special additives at 50°C and pH $\sim$4.2. The nickel growths with a rate of 12 μm/hr until forming a layer of 300 μm. To reinforce the metal insert, a copper layer is deposited on the nickel layer by using as electrolyte, a copper sulphate solution at pH $\sim$0–1. The copper growths with a rate of 40 μm/hr, until forming a layer of 1700 μm.

4. The metal matrix is cut from the Ti wafer by wire cutting. After cutting, a thin Ti film remains on the electroformed PMMA/Ni/Cu system that can be removed either wet chemically at this stage, or

TABLE II Comparison between theoretically selected and actually measured pore dimensions on a fabricated PMMA micro-model

	Depth (μm)		Width (μm)			Depth (μm)		Width (μm)	
Column	Select.	Meas.	Select.	Meas.	Row	Select.	Meas.	Select.	Meas.
1	20	24.1	80	86.0	1	15	16.4	30	39.9
2	5	10.3	15	20.8	3	10	11.3	30	36.7
3	10	11.7	40	47.2	4	15	10.3	15	21.7
4	20	20.0	20	33.5	5	20	19.4	20	31.2
5	15	16.7	30	41.3	6	20	23.8	80	83.8
6	10	11.4	30	39.0	7	20	23.5	60	66.7
8	20	23.5	60	66.7	10	25	28.3	50	52.7
10	15	17.6	45	54.3	11	20	23.7	40	52.7
11	10	9.9	20	24.3	14	15	17.3	60	60.1
12	20	23.5	40	52.3	16	10	9.7	20	24.3
13	20	20.0	20	28.4	17	25	24.8	25	39.9
15	10	10.6	10	14.1	19	10	11.7	40	47.2
17	20	25.2	40	41.3	23	25	26.6	75	79.9
38	25	28.4	50	50.0					

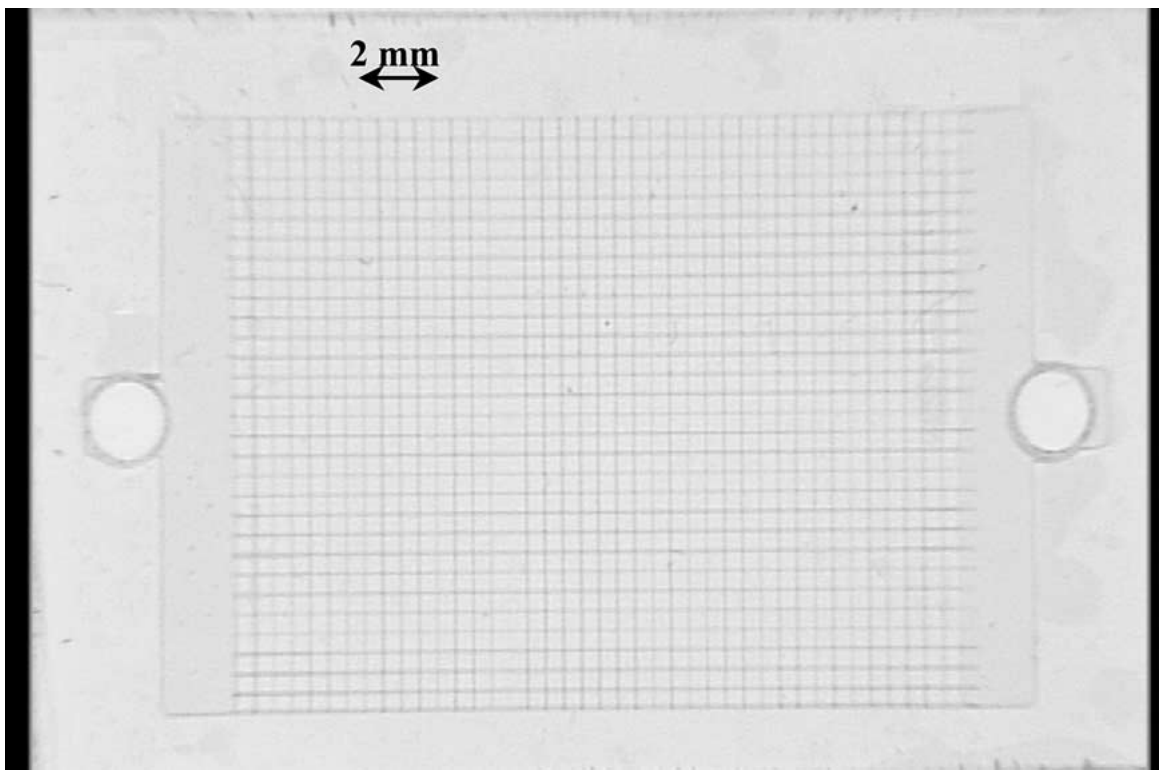

Figure 4 Overview of the entire surface of a pore network micro-model.

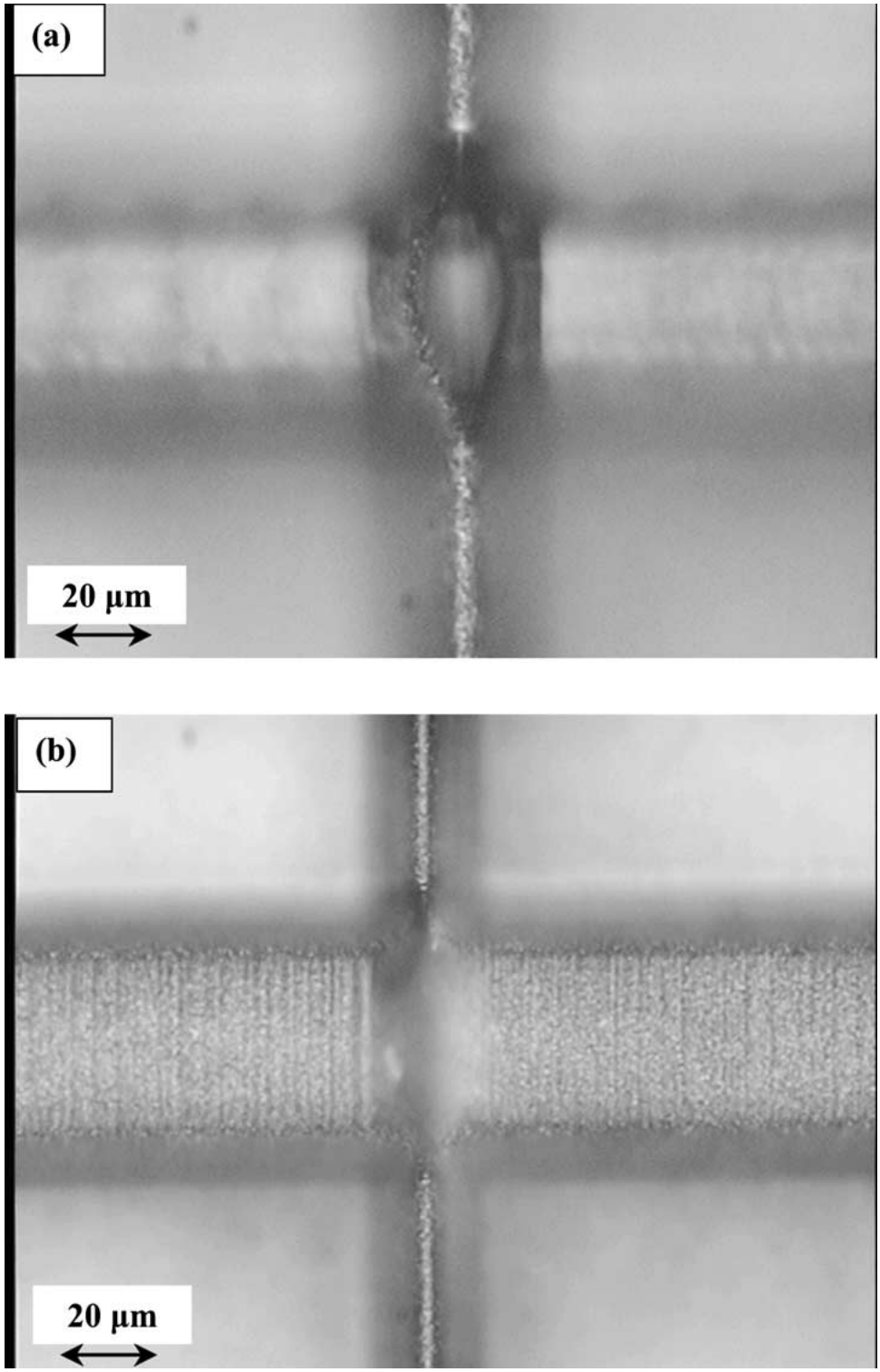

Figure 5 (a) Microscopic detail of an intersection region (node) by focusing on the bottom of the perpendicular adjacent pores. (b) Microscopic detail of the intersection region by focusing on the bottom of the horizontal adjacent pores.

thermo-mechanically during hot embossing. The polymer layer of PMMA is dissolved and the rough surface of the metal matrix is polished mechanically with conventional polishing whereas the insert is cut in its final dimensions with wire cutting.

5. The metal matrix is used as a mould insert and identical PMMA models are constructed from it with hot embossing. Some traces of the titanium remaining on the surface of matrix are removed during this stage. Care is taken to properly adjust the temperature and force in the hot embossing chamber in order to achieve the optimal quality. It was found that a temperature close to 160°C and a force close to 1000 N/m^2 gave the optimal results. The pore depth and width of micromodels are expected to differ slightly from the corresponding input values of the pattern because of imperfections developed during electroforming and bending stresses developed during hot embossing. The pore widths and depths were measured on the final micromodels by using UV-interferometry with the aid of the program WYKO (Fig. 2). The measurements confirmed that there is a small deviation with regard to

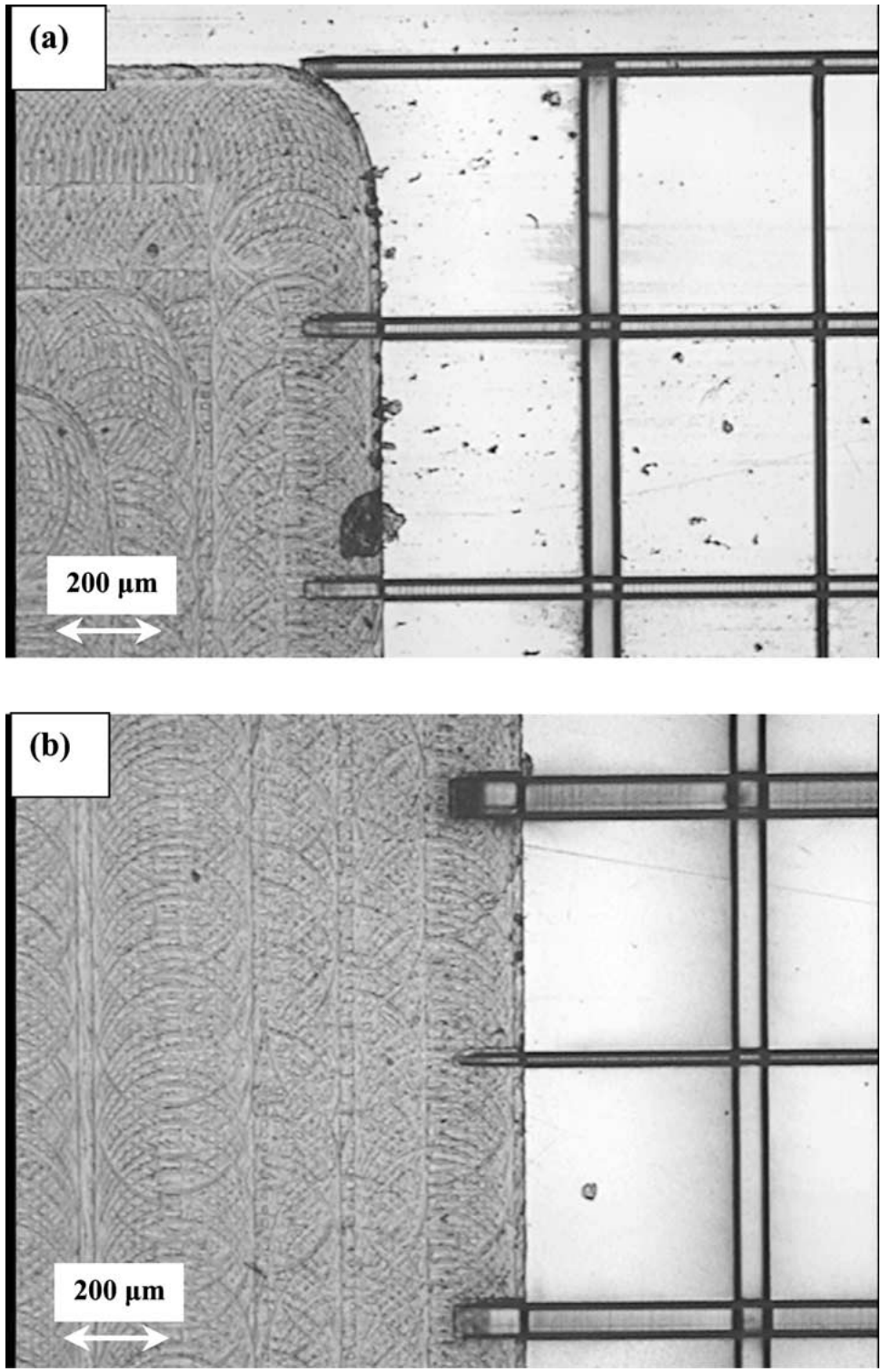

Figure 6 (a) Detail of the connection of the pore network with the trough in a corner region. (b) Detail of the connection of the etched pore network with the trough in the middle region.

pore widths, whereas pore depths remain almost unaltered (Table II). In addition, measurements of the depth of adjacent pores and their intersection region (cross-linkages of a row with a column, Fig. 3) indicated that the depth of each intersection (node) was almost equal to the sum of the depths of the two adjoining pores (bonds) (Table III).

6. Inlet and outlet holes are drilled in the middle of the troughs of each PPMA micromodel. Then a thin PMMA foil (thickness $\sim$125 μm) is glued on the plate of each micromodel by using a spin coating technique. A very thin layer of a glue is spread on the surface of the foil and the etched plastic plate is placed on it. The entire system is centrifuged at a specified revolution rate for a finite time span until a uniform thin layer is formed, and then is left in a UV-oven for several minutes until the glue hardens.

A metal insert and seventeen pore network models (Fig. 4) were constructed by using the excimer laser LIGA process. The quality of the structural characteristics of micromodels was checked before their gluing

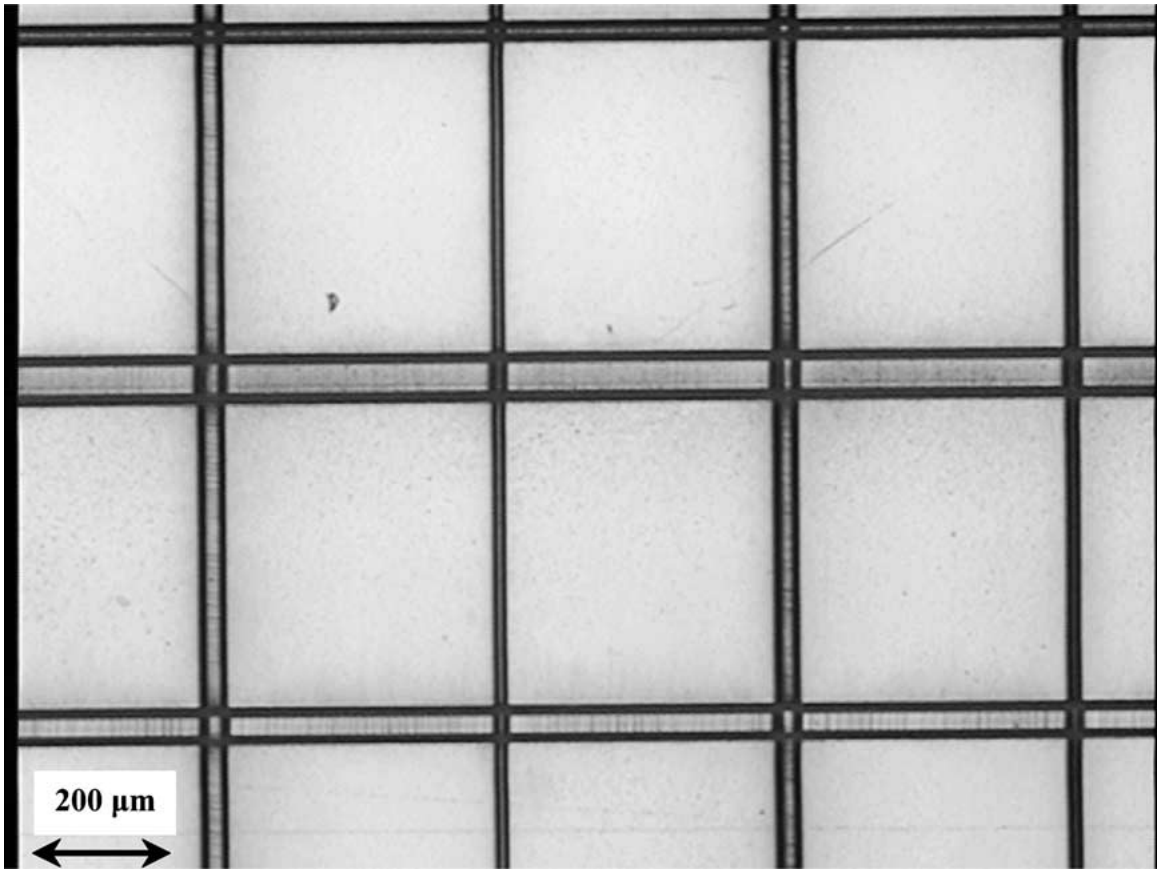

Figure 7 Overview of the fabricated pore network.

with cover foil plates by using optical microscopy and UV-interferometry and was found satisfactory (Figs 5–7). Specifically, any intersection region was always deeper than its adjacent pores (Fig. 5), whereas no discontinuities were formed in the junctions of the pore network with the troughs (Fig. 6a and b).

3. Two-phase flow experiments

Some preliminary two-phase immiscible displacement experiments were performed on the new PMMA pore network models (Fig. 4). Simple imbibition experiments, where the air (non-wetting fluid) occupying the pore space is displaced by n-decane (wetting fluid), were performed (Fig. 8) at two constant inflow rates (250 m1/hr, 500 ml/hr) by using a Harvard Syringe pump (Type: 55-2219). Successive shortcuts of the displacement process were taken by a Camera (Sony) and were directly recorded on a hard disk by using a fully automated real-time digitizer (DPS) that is capable of capturing pictures with a velocity of 25 frames/sec. Time-dependent representative successive short-cuts of a displacement experiment are shown in Fig. 9. After the breakthrough of the invading phase (Fig. 9, shortcut 17) the system tends very fast to steady state (Fig. 9, shortcuts 18–20). In multiphase processes through porous media, the ratio of viscous to capillary forces is expressed by the capillary number Ca [8, 18, 23] which is given by

$$\mathrm{Ca} = \mu u/\sigma \qquad (1)$$

TABLE III Sample measurements of the depth of pores and their junctions (nodes) in two different regions of an unglued and a glued micromodel

Pore element	Region A (unglued model) Mean depth (μm)	Region B (glued model) Mean depth (μm)
Row 1	11.3	15.7
Row 2	15.5	21.1
Column 3	12.6	24.8
Column 4	28.9	11.9
Node a	22.4	39.7
Node b	40.0	26.9
Node c	27.5	45.8
Node d	44.9	31.9

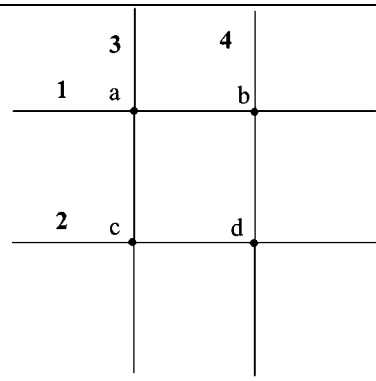

where μ is the viscosity of the invading phase, u is the injection velocity and σ is the interfacial tension of the two fluids.

The depth of each intersection region (node) of pores (bonds) is equal to the sum of the depths of the adjacent intersected pores. Hence, during the displacement of air

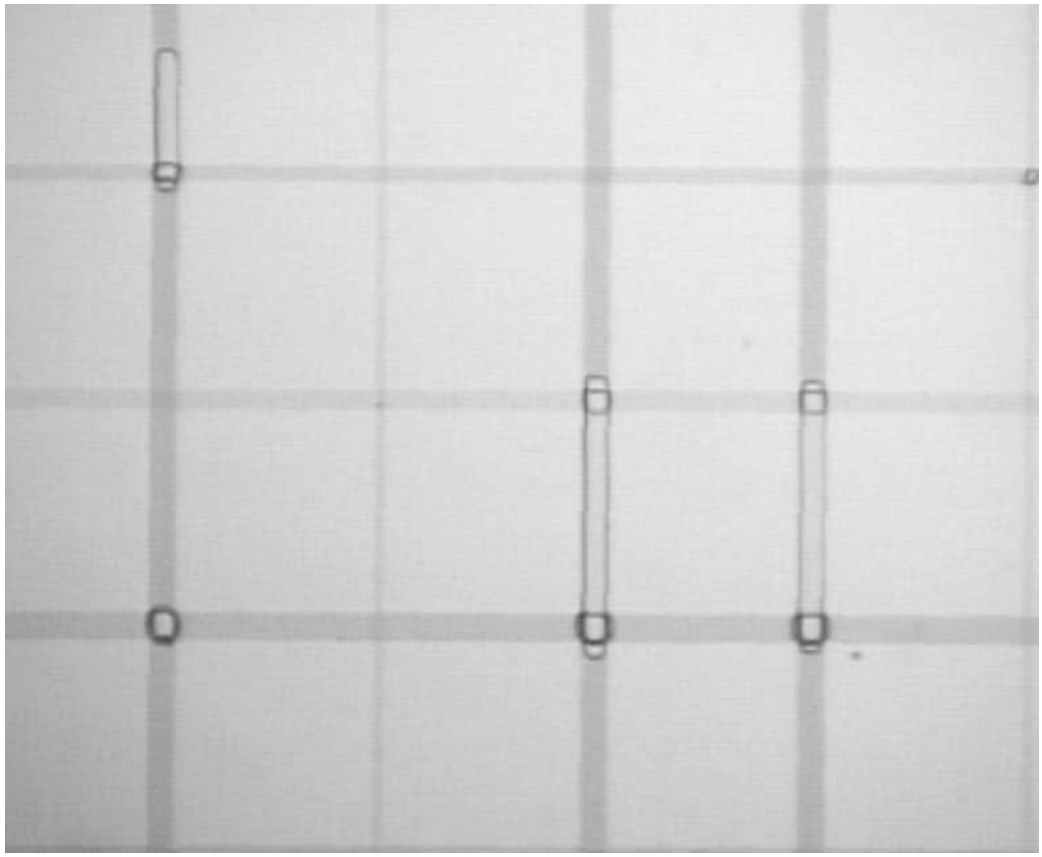

Figure 8 Microscopic detail of a region of the micromodel that is occupied by *n*-decane (dark continuous phase) and air (light isolated blobs).

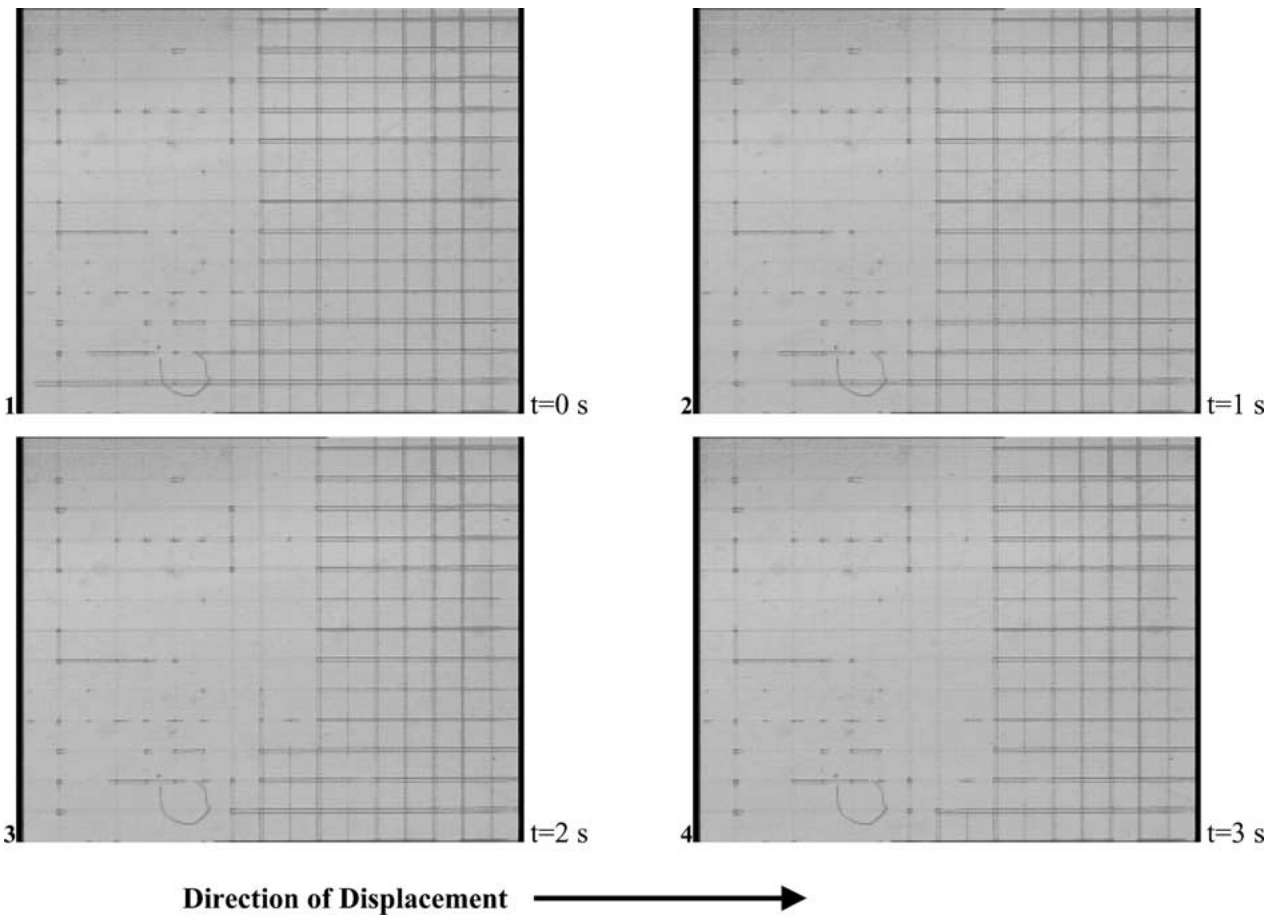

Figure 9 Successive shortcuts of the immiscible displacement of air by *n*-decane at capillary number $Ca = 10^{-6}$. (*Continued*.)

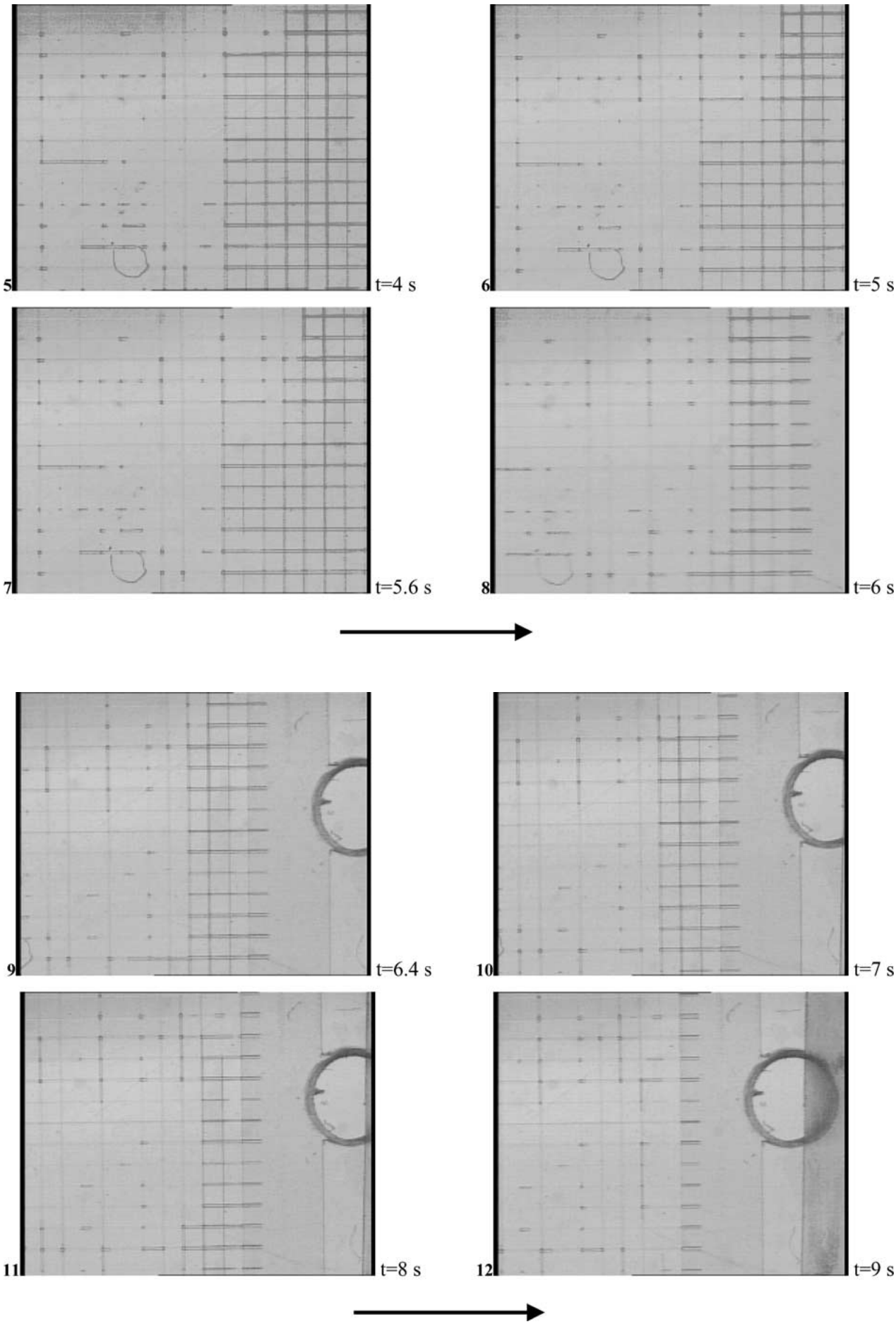

Figure 9 (*Continued.*)

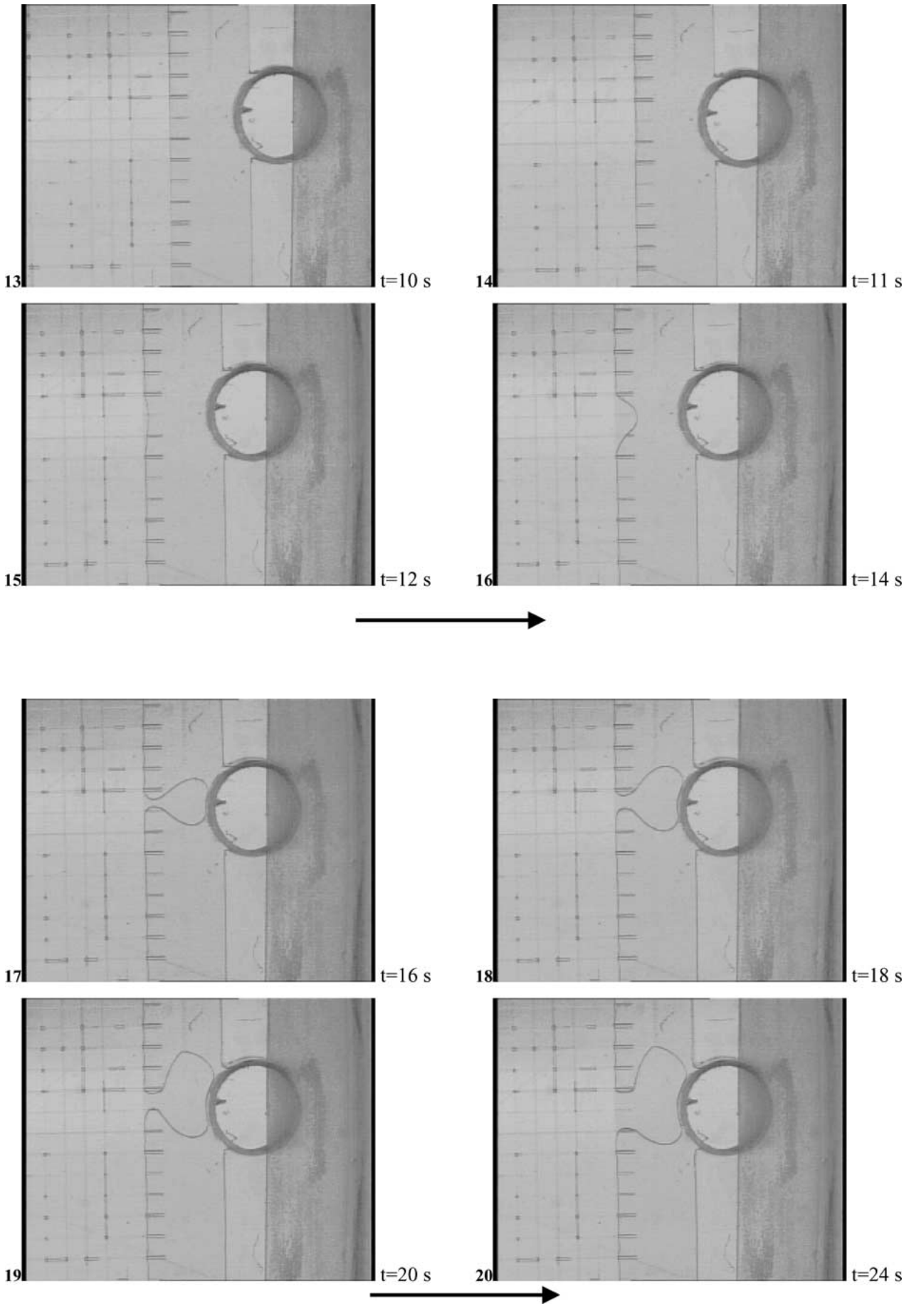

Figure 9 (*Continued.*)

from n-decane, the capillary pressure exerted on interfaces encountered in pores (bonds) is always greater than that exerted on interfaces created in intersection regions (nodes). So, the filling of the pores (bonds) with the wetting fluid is favored against the filling of the intersection regions (nodes). For this reason, most ganglia of the non-wetting fluid are trapped in intersection regions (Fig. 9) rather than in pore clusters, as it usually occurs during displacement experiments in conventional glass-etched models [8, 11, 18, 20, 21, 23].

4. Conclusions

Pore network micro-models were fabricated on transparent plastic PMMA plates by using a new method based on the excimer laser LIGA technique. A metal moulding insert was first fabricated through excimer laser ablation and electroforming, then a large number of identical plastic etched micro-models was replicated by using a hot embossing technique, and finally each model was glued with a cover thin foil with spin coating. The pore network models are intended to be used in visualization experimental studies of multiphase flow through porous media. Measurements of the structural characteristics of the micromodels confirmed their improved features against the older ones produced by using wet chemistry techniques. Specifically, the new models exhibit well-controlled pore depth and width distributions, a broad pore depth range which is by one order of magnitude ($\sim$20 μm) lower than that of the conventional glass models ($\sim$100 μm), and pore intersection regions (nodes) deeper than their adjacent pores (bonds). In this manner, the capillary properties of the new models are expected to be close to those of prototype porous media such as natural formations (e.g. sedimentary rocks, soils, etc). The applicability of the new models to multiphase transport studies was confirmed by performing certain preliminary air/n-decane immiscible displacement experiments on them.

Acknowledgements

The fabrication of micro-structures was performed at the Institute of Microtechnology Mainz (IMM), Germany, under a Guest Experiment granted by IMM to ICE/HT-FORTH (Sub-Project Contract No: P-95047-14) as a part of an EC-funded Large Scale Facility (LSF) Project of IMM (Contract No: ERB-FMGE-CT98–0138). All staff of IMM is acknowledged for its hospitality, collaboration and contribution to the various stages of micro-fabrication processes. Special thanks are due to Dr. Thomas Stange, Dr. Thomas Klotzbuecher, Mr. Thorsten Braune, Mr. Sven Krueger, Dr. Raimund Broechler and Mr. Johannes Ott for the fruitful discussions and their valuable assistance during all phases of the project.

References

1. M. BLUNT, M. J. KING and H. SCHER, *Phys. Rev. A* **46** (1992) 7680.
2. I. CHATZIS and F. A. L. DULLIEN, *J. Can. Pet. Technol.* **16** (1977) 97.
3. F. A. L. DULLIEN, "Porous Media: Fluid Transport and Pore Structure" (Academic Press, San Diego, California, 1992).
4. A. C. PAYATAKES and M. M. DIAS, *Rev. Chem. Eng.* **2** (1984) 85.
5. M. SAHIMI, *Rev. Mod. Phys.* **65** (1993) 1393.
6. M. A. CELIA, J. S. KINDRED and I. HERRERA, *Water Resour. Res.* **25** (1989) 1141.
7. T. F. RUSSEL, *Rev. Geophys.* (Suppl.) (July 1995) 1035.
8. D. G. AVRAAM, G. B. KOLONIS, T. C. ROUMELIOTIS, G. N. CONSTANTINIDES and A. C. PAYATAKES, *Transp. Porous Media* **16** (1994) 75.
9. J. S. BUCKLEY, in "Interfacial Phenomena in Petroleum Recovery" (Marcel-Dekker, New York, 1991) p.157.
10. S. H. CONRAD, J. L. WILSON, W. R. MASON and W. J. PEPLINSKI, *Water Resour. Res.* **28** (1992) 467.
11. M. A. IOANNIDIS, I. CHATZIS and A. C. PAYATAKES, *J. Colloid Interface Sci.* **143** (1991) 22.
12. A. A. KELLER, M. J. BLUNT and P. V. ROBERTS, *Transp. Porous Media* **26** (1997) 277.
13. R. LENORMAND, C. ZARCONE and A. SARR, *J. Fluid Mech.* **135** (1983) 337.
14. Y. LI and N. C. WARDLAW, *J. Colloid Interface Sci.* **109** (1986) 473.
15. W. E. SOLL, M. A. CELIA and J. L. WILSON, *Water Resour. Res.* **29** (1993) 2963.
16. C. D. TSAKIROGLOU, G. B. KOLONIS, T. C. ROUMELIOTIS and A. C. PAYATAKES, *J. Colloid Interface Sci.* **193** (1997) 259.
17. N. C. WARDLAW and Y. LI, *Transport in Porous Media* **3** (1988) 17.
18. D. G. AVRAAM and A. C. PAYATAKES, *J. Fluid Mech.* **293** (1995) 207.
19. R. LENORMAND, E. TOUBOUL and C. ZARCONE, *ibid.* **189** (1988) 165.
20. C. D. TSAKIROGLOU and A. C. PAYATAKES, *Adv. Colloid Interface Sci.* **75** (1998) 215.
21. O. VIZIKA, D. G. AVRAAM and A. C. PAYATAKES, *J. Colloid Interface Sci.* **165** (1994) 386.
22. J. WAN and J. L. WILSON, *Water Resour. Res.* **30** (1994) 11.
23. D. G. AVRAAM and A. C. PAYATAKES, *Ind. Eng. Chem. Res.* **38** (1999) 778.
24. I. CHATZIS, N. R. MORROW and H. T. LIM, *Soc. Pet. Eng.* **23** (1983) 311.
25. M. BLUNT, *J. Pet. Sci. Eng.* **20** (1998) 117.
26. G. N. CONSTANTINIDES and A. C. PAYATAKES, *AIChE J.* **42** (1996) 369.
27. C. D. TSAKIROGLOU and A. C. PAYATAKES, *Adv. Water Resour.* **23** (2000) 773.
28. J. ARNOLD, U. DASBACH, W. EHRFELD, K. HESCH and H. LOEWE, *Appl. Surf. Sci.* **86** (1995) 251.

Received 8 September 2000
and accepted 3 August 2001